Submitted, accepted and published by:
Fuel 195 (2017) 38-48

Titanium Substituted Manganese-Ferrite as an Oxygen Carrier with Permanent Magnetic Properties for Chemical Looping Combustion of Solid Fuels

María Abián, Alberto Abad*, María T. Izquierdo, Pilar Gayán, Luis F. de Diego, Francisco García-Labiano, Juan Adánez

Instituto de Carboquímica (ICB-CSIC), Miguel Luesma Castán, 4, Zaragoza, E-50018, Spain.

Corresponding author: *Phone: + 34 976 733 977. Fax: +34 976 733 318. E-mail: abad@icb.csic.es

Abstract

Mixed oxides of Mn-Fe have been identified as suitable materials for Chemical Looping Combustion (CLC) with solid fuels both via *in-situ* Gasification Chemical Looping Combustion (*i*G-CLC) and Chemical Looping with Oxygen Uncoupling (CLOU) processes. These materials show the property of react with gaseous fuels as well as release oxygen under given conditions, while cheap metals are used. In addition, these materials can show magnetic properties that can be used for an easy separation from ash in CLC with solid fuels. Thus, losses of oxygen carrier material in the ash drain stream would be reduced. Different cations have been proposed for improving the magnetic properties of manganese ferrites, including Ti^{4+}. In this context, the present work accomplishes a screening of $(Mn_xFe_{1-x})_2O_3$ doped with 7 wt.% TiO_2, with x ranging from 0 to 1. The influence of Mn:Fe ratio on their physical and chemical properties was evaluated. In general, particles with high crushing strength values (>4 N) were obtained, and magnetic characteristics were highlighted when $x \leq 0.66$. The oxygen uncoupling capability depended on the Mn:Fe ratio and the oxidation conditions, i.e. temperature and oxygen partial pressure. Broader oxidation conditions to take advantage of the oxygen uncoupling capability were found for materials with low Mn content. On contrary, the reactivity with fuel gases (CH_4, H_2 and CO) increased with the Mn content. Thus, oxygen carriers with Mn/(Mn+Fe) molar ratio in the 0.5-0.9 interval showed interesting properties at suitable temperatures for the *i*G-CLC and CLOU processes (i.e. 850-980 ºC). The material with Mn/(Mn+Fe) = 0.55 was preferred considering a trade-off between reactivity and magnetic properties.

Keywords: CO_2 capture, Chemical Looping Combustion, Oxygen carrier, Manganese oxide, Iron oxide.

Submitted, accepted and published by:
Fuel 195 (2017) 38-48

1. Introduction

Nowadays, research involving the reduction of net CO_2 emissions to the atmosphere from combustion systems is still a challenge. Emerging combustion processes with intrinsic CO_2 capture, such as Chemical Looping Combustion (CLC), are of increasing interest since no energy or equipment is needed for gas separation as compared with the classic CO_2 capture systems (pre, post and oxyfuel combustion) [1]. Chemical Looping Combustion (CLC) implies the use of an oxygen carrier, generally a metal oxide, to transfer the oxygen from the air to the fuel. A CLC system basically consists of two interconnected fluidized beds, namely fuel and air reactors, with a particulate oxygen carrier continuously circulating between them [2]. In the fuel reactor, the fuel is combusted taken oxygen from the oxygen carrier, while the oxygen carrier is re-oxidized with air in the air reactor. Thus, the direct contact between fuel and air is avoided and, the CO_2 capture is inherent to the CLC process.

Mainly, the use of solid fuels in CLC is being developed by two different approaches: *in-situ* Gasification Chemical Looping Combustion (*i*G-CLC) and Chemical Looping with Oxygen Uncoupling (CLOU) [3]. In *i*G-CLC, the solid fuel is gasified by steam and/or carbon dioxide; then the generated gaseous products (mainly CO, H_2 and CH_4) react with the oxygen carrier to produce the combustion products (CO_2 and H_2O). When coal is considered the fuel, loss of oxygen carrier particles is expected in the drainage flow of ash. Thus, low cost materials such as ilmenite [4-6], iron ore [7-9], manganese ore [10] or waste materials [11] have been mostly evaluated for *i*G-CLC in pilot units up to 1 MW_{th}. In these cases, high CO_2 capture was achieved, but complete combustion was not reached [12]. In CLOU, the oxygen carrier is able to evolve gaseous oxygen in the fuel reactor, thus allowing the combustion of the solid fuel with O_2. The CLOU process was proposed by Mattisson et al. [13] to improve the combustion of solid fuels. Then, the proof of the concept was performed in a 1.5 kW CLOU unit by Abad et al. [14]. High CO_2 capture rates with complete combustion of different solid fuels (coal, lignite, biomass) was achieved by using a Cu-based oxygen carrier [14-16].

Alternatively to Cu-based materials, Mn-Fe mixed oxides have been identified as suitable materials for CLOU, while cheap and environmental friendly metals are used [17]. Bixbyite phase, $(Mn_xFe_{1-x})_2O_3$, must be formed during oxidation in order to show oxygen uncoupling capability during reduction to spinel phase,

$(Mn_xFe_{1-x})_3O_4$ [18]. Thus, coal combustion was improved by taking advantage of the oxygen uncoupling capability of bixbyite when oxidation in the air reactor was optimized [19]. In addition, spinel phase $(Mn_xFe_{1-x})_3O_4$ can be reduced by fuel gases (e.g. H_2, CO, CH_4) to manganowüstite $(Mn_xFe_{1-x})O$, thus being active for *i*G-CLC [20-23].

The influence of the Mn:Fe ratio on the suitability of Mn-Fe mixed oxides for CLOU have been evaluated in the literature [21-25]. In general, oxygen carriers with Mn:Fe ratios higher than 0.6 show better fuel gas conversion and oxygen uncoupling capability at lower temperature (850 ºC) than oxygen carriers with lower Mn:Fe ratios. But the potential for the oxidation to bixbyite improved as the Mn:Fe ratio was decreased [23]. i.e. they can be oxidized at higher temperatures, e.g. 950 ºC, than materials with high Mn:Fe ratio.

Although manganese and iron can be considered as cheap materials, Mn-Fe mixed oxide materials must be synthetized, thus increasing its prize compared to low-cost materials such as natural ores. Therefore, it would be very interesting the recovering of lost oxygen carrier particles with the ash. In this sense, Mn-Fe mixed oxides show magnetic properties in the spinel phase [26, 27], which could be used for a magnetic separation from ash. In addition, different cations have been proposed for improving the magnetic properties of manganese ferrites, e.g. by dopping Mn-Fe mixed oxides with Ti^{4+} [28]. However, the magnetic properties of Mn-Fe mixed oxides in oxygen carriers for chemical looping applications have been not studied.

An oxygen carrier should accomplish the following characteristics: sufficient oxygen capacity, favorable thermodynamics regarding the fuel conversion to CO_2 and H_2O, high reactivity for reduction and oxidation reactions maintaining it during many successive redox cycles, resistance to attrition, negligible carbon deposition, good fluidization properties and environmental friendly characteristics [3]. In a previous work, Fe-Mn mixed oxides particles were obtained by mechanical mixing of Mn_3O_4 and Fe_2O_3 powders (Mn:Fe molar ratio of 0.77:0.33), which showed relatively high reactivity and crushing strength values (> 1N) [29]. Also, particles were prepared by doping with TiO_2 a material prepared by spray drying with Mn:Fe molar ratio of 0.66:0.34. These particles were successfully tested in a continuously operated CLC unit burning coal [19].

In this context, in the present work a screening of the performance of Mn-Fe-Ti based oxygen carriers, prepared with different Mn:Fe molar ratios and a fixed TiO_2 concentration, is performed. The characterization of the oxygen carriers has been based on the evaluation of their mechanical strength, the reduction and

oxidation rates through TGA experiments at temperatures suitable for the *i*G-CLC and CLOU processes (i.e. 850-950 ºC), and the determination of the magnetic susceptibility of the particles as a reference value to evaluate the applicability of the magnetic separation from ash.

2. Experimental

2.1. Oxygen Carriers

The oxygen carrier particles were prepared using as raw materials Mn_3O_4 (Strem Chemical, Inc), Fe_2O_3 (Panreac, Prs), and TiO_2 (Panreac, Prs), all of them in powder. The mass fraction of TiO_2 was fixed to 7 wt.%, which was the fraction used in a previous tested material [19], but the Mn:Fe molar ratio was varied in a broad interval; see Table 1. To prepare the oxygen carriers, the reactants, in their respective mass fractions, were firstly ball-milled for 30 min and subsequently pelletized by pressure in a hydraulic press at 160 bar for 60 s, obtaining cylindrical pellets of about 1 cm in diameter and 3 cm in length. The pellets were further calcined at 1200 ºC in a muffle furnace during 2 hours both, to increase the mechanical strength of the particles and to provide the material with permanent magnetic properties, considering results showed in [30]. In some cases, calcination at higher temperatures was required to provide magnetic properties. After calcination, materials with a general formula $Mn_xFe_{1-x}Ti_yO_z$ were obtained. Finally, the pellets were crushed and sieved to obtain particles with a particle diameter of 100-300 μm.

Table 1. Chemical composition, calcination temperature, crushing strength, magnetic permeability and main phases (XRD) of the oxygen carriers.

Oxygen carrier*	**Mn/(Mn+Fe) molar ratio**	**Mass fraction Mn_3O_4:Fe_2O_3:TiO_2**	**T_{calc} (ºC)**	**Crushing strength (N)**	**Magnetic permeability (-)**	**Main phases**
FeTi7	0.00	0:93:7	1200	3.8	1.0	Fe_2O_3 Fe_2TiO_4
Mn28FeTi7	0.28	25:68:7	1200	5.8	5.8	$Mn_{1.03}Fe_{1.97}O_4$ Mn_2FeO_4 Fe_2O_3 $Fe_{1.5}Ti_{0.5}O_3$
Mn55FeTi7	0.55	50:43:7	1200	4.3	8.3	Mn_2FeO_4 $Mn_3Fe_3O_8$ Fe_2TiO_4
Mn66FeTi7	0.66	60:33:7	1200	3.8	7.8	Mn_2FeO_4 $Mn_{1.58}Fe_{1.42}O_4$ Fe_2TiO_4
Mn87FeTi7	0.87	80:13:7	1200 1300 1350 1400	4.7 4.4 4.5 5.4	1.0 1.2 1.2 1.2	Mn_2FeO_4 Mn_3O_4 $FeTiO_4$

MnTi7	1.00	93:0:7	1200 1400	5.1 4.8	1.0 1.0	Mn_2O_3 Mn_3O_4 $MnTiO_3$
* The nomenclature shows the stoichiometric coefficient x and y in the general formula $Mn_xFe_{1-x}Ti_yO_z$						

The crushing strength of the particles was measured using a Shimpo FGN-5X crushing strength apparatus. The value reported for each oxygen carrier is the average value of 20 measurements of the force needed to fracture a particle. The magnetic permeability was measured using a Bartington single frequency MS2G sensor connected to a magnetic susceptibility MS3 meter. Additional information about the determination of magnetic permeability is shown in the Supplementary material S1.

The main phases of the Mn-Fe-Ti system were identified through characterization by X-ray diffraction (XRD). The XRD analysis was performed using a Bruker D8 Advance X-ray powder diffractometer equipped with an X-ray source with a Cu anode working at 40 kV and 40 mA and an energy-dispersive one-dimensional detector. In particular, the diffraction pattern was obtained with a scanning rate of 0.019º over the 2θ range of 10º to 80º, and the assignation and quantification of crystalline phases was performed through the use of the DIFFRAC.EVA and TOPAS software, on base of Joint Committee on Powder Diffraction Standards. The XRD results correspond to the analysis of the oxygen carrier particles obtained after the calcination of the pellets at 1200 ºC.

The oxidation state of Fe, Mn and Ti was studied by XPS in an ESCAPlus Omicron spectrometer equipped with a non-monochromatized MgKα radiation (1253.6 eV). The hemispherical electron energy analyzer was operated at pass energy of 50 eV for surveys, and 20 eV for high-resolution spectra. Binding energies (BE) were referenced to the C1s peak (284.5 eV) from adventitious carbon contamination. Current region sweeps for O1s, Fe 2p, Ti2p, Mn2p and Mn3s were obtained. The CASA data processing software allowed smoothing, background subtraction, peak fitting and quantification.

2.2. Thermogravimetric analyzer (TGA) and procedure

The experiments were performed in a thermogravimetric analyzer (TGA CI Electronics). The detailed description of the TGA and procedure can be found elsewhere [31] and therefore only a brief description is given here. The oxygen carrier mass and gas flow used in the TGA experiments were chosen to avoid limitations in the external film mass-transfer and/or inter particle diffusion. For each test, around 50 mg of oxygen carrier particles were loaded in a platinum wired mesh basket and heated up to the desired temperature

(850, 900 or 950ºC) in an air atmosphere. After stabilization, the oxygen carrier particles were exposed to five successive reduction-oxidation cycles. Both, reduction and oxidation periods were, respectively, 30 minutes. Reduction was carried out with H_2 (5 % H_2 + 40 % H_2O), CO (15 % CO + 20 % CO_2) or CH_4 (15 % CH_4 + 20 % H_2O). A lower concentration was used with H_2 in order to avoid reduction of iron oxide to metallic iron, which is not interesting for CLC [32]. In addition, the oxygen uncoupling capability was evaluated by exposing the solid sample to an inert environment (100 % N_2). The oxidation was carried out either in air or 5 vol.% O_2. A gas flow of 25 L/h (STP) was used in all cases. In general, except for the first cycle, no significant changes in the reactivity to the fuel gases, neither in the oxygen carrier regeneration, were observed through the successive redox cycles. All the results shown in the present work correspond to the third redox cycle.

3. Results

3.1. Phase diagram of the Mn-Fe-Ti-O system

The phase diagrams for different Mn:Fe ratio in the Mn-Fe-Ti-O system as function of the temperature and oxygen partial pressure are shown in Figures 1(a) and 1(b), respectively. FToxid database from the FactSage software was used [33]. According to the phase diagrams shown in Figure 1, seven phases in the $(Mn_xFe_{1-x})Ti_{0.15}O_z$ system are thermodynamically stable, which are distributed in different regions depending upon the given oxygen partial pressure, temperature and the Mn:Fe ratio.

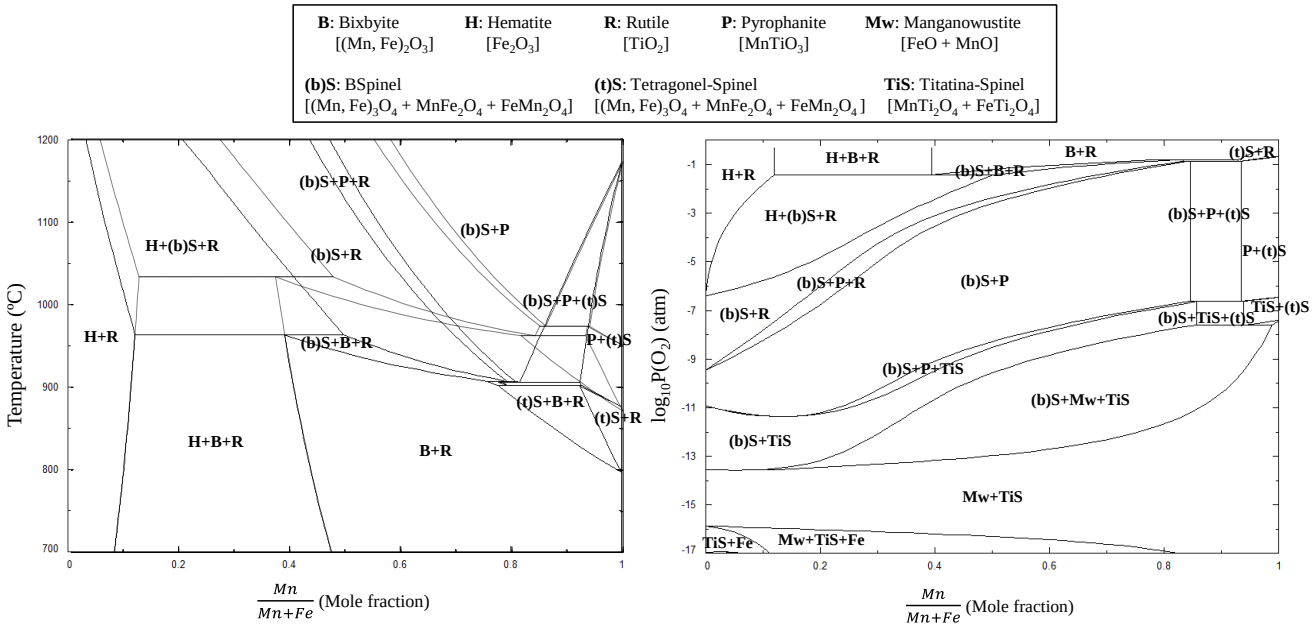

Figure 1. Phase diagram of the $(Mn_yFe_{1-y})Ti_{0.07}O_x$ system as function of the Mn-Fe composition and (a)

temperature in either 0.05 (solid lines) or 0.21 atm O_2 (dot lines), and (b) partial pressure of O_2 at 950 ºC.

Focused in the oxidation of Mn-Fe mixed oxides, equilibrium conditions at the air reactor exit are evaluated in Figure 1(a); that is in 5 vol.% O_2 assuming 25 vol.% of air excess, similar to the excess used in conventional combustion. In general, low temperature regions are dominated by bixbyite phases, while spinel phase appear in the upper temperature region. The temperature for the bixbyite to spinel transformation monotonically decreases from the transformation temperature for Fe_2O_3/Fe_3O_4 (1600 ºC) to Mn_2O_3/Mn_3O_4 (800 ºC) as the Mn:Fe ratio increases. In the lower temperature regions, the hematite Fe_2O_3 and rutile TiO_2 phases coexist for Mn contents lower than about 0.1. At increased Mn ratios bixbyite phase appears separated from Ti-containing phases at the expense of the hematite phase; eventually bixbyite and rutile coexist as separated phases for Mn/(Mn+Fe) ratios higher than 0.4-0.48. At higher temperatures, bixbyite or hematite is completely transformed to spinel. Rutile and β-spinel dominates the regions with lower Mn content, while pyrophanite (i.e. the manganese rich ilmenite $MnTiO_3$) and tetragonal spinel appear as the Mn content increases.

3.2. Crushing strength, XRD and magnetic permeability evaluation

The crushing strength of all the particles prepared in the present work are around 4-5 N; see Table 1. A minimum of 3.8 N was obtained for Mn66FeTi7, and the crushing strength was monotonically increased as the Mn content either increased or decreased, excepting for FeTi7 that showed a crushing strength of 3.8 N. Similar results were obtained by Azimi et al. [24], but higher crushing strength values are here obtained. Different preparation method, calcining temperature or the presence/avoidance of Ti can be argued to justify the different crushing strength here obtained. However, similar particles but without Ti showed crushing strength values around 2-3 N [29], suggesting that the improvement here shown could be mainly attributed to the presence of Ti. Usually, oxygen carriers with a crushing strength above 1-2 N [34,35] have been identified in previous works to be more likely resistant to attrition in continuous operation, which points to the potential of these Mn-Fe-Ti based oxygen carriers for providing a good mechanical stability for CLC applications. This is an interesting result since the material screening will not be conditioned by the mechanical strength of the particles, but to the analysis of the effect of Mn:Fe ratio on the redox kinetics and the magnetic properties.

The revealed phases by XRD and magnetic permeability values resulted a function of the Mn-Fe relation and the calcination temperature. Thus, only the oxygen carriers with Mn/(Mn+Fe) molar ratios between 0.28 and 0.66 showed magnetic properties when they were calcined for 2 h at 1200 ºC, with magnetic permeability values in the 5.5-8.5 interval. These particles were characterized by the presence of Mn-Fe mixed oxides in the spinel form, i.e. $(Mn_xFe_{1-x})_3O_4$. Calcination conditions promoted the formation of the spinel phase (see Figure 1), which was not oxidized to bixbyite phase, $(Mn_xFe_{1-x})_2O_3$, during the cooling stage after calcination of the pellets in air. It is well known the magnetism showed by the Mn-Fe spinel [27-29], which justify this result. Nevertheless, the oxygen carrier particles are partially oxidized to bixbyite phase during the oxidation tests in TGA. Rutile, TiO_2, was not detected by XRD, but rather Fe-Ti mixed oxides were formed.

For the Mn87FeTi7 material, limited formation of spinel phase was observed because of the low iron content regardless the calcination temperature, but in any case bixbyite was not detected. However, magnetic permeability was raised from 1.0 to 1.2 when calcining temperature was increasing from 1200 to 1400 ºC. Therefore, the existence of magnetic properties is not only guaranteed by the presence of spinel phase, but also another factor should be considered. The reason for the effect of calcining temperature on the magnetic permeability could be found in the shifting of the following equilibrium:

$$Mn^{3+} + Fe^{2+} \leftrightarrow Mn^{2+} + Fe^{3+} \quad \text{(R1)}$$

In a Mn-rich spinel, the spinel structure would show the following general distribution of cations: $\left[Mn^{3+}_{1-x}Fe^{2+}_{x}\right]_A\left[Mn^{3+}_{1+x}Fe^{2+}_{1-x}\right]_B O_4$; where subscripts "A" and "B" denote tetrahedral and octahedral sites, respectively [CITA??]. In fact, XPS results revealed that Mn is in the Mn^{3+} oxidation state for the Mn87FeTi7 material when the calcining temperature is 1200 ºC. However, XPS analysis revealed the presence of both Mn^{3+} and Mn^{2+} in the samples calcined at higher temperatures (i.e. 1300, 1350 and 1400 ºC), which means that part of the Mn^{3+} is transformed to Mn^{2+}. Consequently, some Fe^{2+} should be transformed into Fe^{3+}, according to equilibrium (R1). The variation in the oxidation state of Mn and Fe modifies their disposition in the crystal structure, which also modifies the magnetic permeability of the material [28].

Taking into account XRD, XPS and magnetic permeability results, the following theory is postulated to address the magnetic behavior of Mn87FeTi7 material as function of the calcining temperature. Mn87FeTi7 calcined at 1200 ºC would show the $\left[Mn^{3+}_{1-x}Fe^{2+}_{x}\right]_A\left[Mn^{3+}_{1+x}Fe^{2+}_{1-x}\right]_B O_4$ spinel structure, which does not show

magnetic properties. The calcination at a higher temperature promoted the presence of Mn^{2+} and Fe^{3+} at the expense of Mn^{3+} and Fe^{2+} both in the tetrahedral and octahedral sites leading to the formation of $\left[Mn^{3+}_{1-x-y}Mn^{2+}_{y}Fe^{2+}_{x-y}Fe^{3+}_{y}\right]_A\left[Mn^{3+}_{1+x-z}Mn^{2+}_{z}Fe^{2+}_{1-x-z}Fe^{3+}_{z}\right]_B O_4$. The presence of Fe3+ ions both in the tetrahedral and octahedral sites provides magnetic properties to the spinel structure [CITAS]. Thus, a higher calcining temperature could result in higher magnetic properties.

On the contrary, neither the ilmenite surrogate (FeTi7) nor the Mn-Ti based oxygen carrier (MnTi7) showed magnetic behavior independently on the calcination temperature (1200 to 1400 ºC). In these cases, the presence of Mn_2O_3 and/or Mn_3O_4 is highlighted. In addition, pyrophanite, $MnTiO_3$, was detected by XRD, according to the phase diagram in Figure 1.

As a conclusion, high values of the magnetic permeability correspond to a ferrimagnetic behavior, and thus would allow an easy separation of these carriers from the ashes. This property can be exploited for particles with Mn/(Mn+Fe) ratios between 0.28 and 0.66. Particles calcined at 1200 ºC were selected for further testing and characterization, with the exception of Mn87FeTi7 which was calcined at 1300 ºC.

3.3. Oxygen transport capacity

The typical reaction involving the oxygen release for CLOU in these materials is the decomposition of bixbyite ($(Mn_xFe_{1-x})_2O_3$) to spinel ($(Mn_xFe_{1-x})_3O_4$. Thus, bixbyite should be formed to take advantage of the oxygen uncoupling capability of these materials; see reaction R1.

$$3\,(Mn_xFe_{1-x})_2O_3\ \textit{(bixbyite)} \leftrightarrow 2\,(Mn_xFe_{1-x})_3O_4\ \textit{(spinel)} + 0.5\,O_2\ \textit{(g)} \qquad \text{(R2)}$$

Between bixbyite and spinel phases there is a miscibility gap where bixbyite and spinel phases co-exist; see Figure 1. This region is especially relevant for Mn/(Mn+Fe) < 0.5. However, the miscibility gap is characterized by a low temperature difference for Mn/(Mn+Fe) ratios in the 0.5-0.8 interval.

It is very interesting to note that a fraction of the Mn can also evolve oxygen via the formation of pyrophanite, $MnTiO_3$, in the presence of Ti; see reactions R3 and R4 –additional information about the determination of coefficients b, c and y in reactions R3 and R4 is shown in the Supplementary material S2–. This fact is especially relevant for Mn/(Mn+Fe) > 0.8, when this transformation can occur at the vicinity of 900 ºC. However, for materials with high Mn content, bixtyite in the form of Mn_2O_3 only would be formed at a temperature lower than 800 ºC, which is not a temperature of interest for CLC with solid fuels.

227 $(Mn_xFe_{1-x})_2O_3$ *(bixbyite)* + a TiO_2 ↔ a $MnTiO_3$ *(pyrophanite)* + b $(Mn_yFe_{1-y})_3O_4$ *(spinel)* + c O_2 *(g)*(R3)

228 $(Mn_xFe_{1-x})_3O_4$ *(spinel)* + a TiO_2 ↔ a $MnTiO_3$ *(pyrophanite)* + b' $(Mn_{y'}Fe_{1-y'})_3O_4$ *(spinel)* + c' O_2 *(g)*(R4)

229 In addition, Mn-Fe mixed oxides can be highly reduced to manganowüstite, $Mn_xFe_{1-x}O$, in the presence of a
230 fuel gas, e.g. H_2, CO or CH_4 [21]. To evaluate this issue, the phase diagram as a function of the oxygen partial
231 pressure is presented; see Figure 1(b). Regions in the upper oxygen pressure values are characterized by
232 bixbyite rich phases. As the oxygen partial pressure decreases, spinel rich phases are formed, following
233 reaction R2. As well, pyrophanite is formed for highly Mn-rich material following reactions R3 or R4. In
234 these cases, the oxygen uncoupling capability can be used due to these reactions take place spontaneously in
235 the fuel reactor where oxygen partial pressure is low. But manganowüstite, i.e. the more reduced phase
236 $Mn_xFe_{1-x}O$, is formed at lower oxygen partial pressures. For practical purposes, this phase would be formed in
237 the presence of a reducing gas.
238 Considering re-oxidation in the air reactor, spinel phase can be easily formed at the air reactor conditions.
239 However, to take advantage of the oxygen uncoupling potential during successive cycles in the CLC system,
240 bixbyite needs to be effectively formed at the conditions of the air reactor via reverse of reaction R2. At the
241 relatively low partial pressure (5 vol.% O_2) the bixbyite regeneration is allowed for Mn/(Mn+Fe) molar ratios
242 lower than 0.5 at 950 ºC. For higher Mn/(Mn+Fe) ratios a higher oxygen partial pressure or lower temperature
243 would be required to form bixbyite; see Figure 1.
244 From the above analysis it is concluded that oxygen carrier can be oxidized to bixbyite at suitable O_2 partial
245 pressure and temperature conditions. Then, bixbyite can transfer oxygen via oxygen uncoupling by reduction
246 to spinel, and a further reduction to manganowüstite can be exploited by reaction with a fuel gas. To evaluate
247 the fraction of available oxygen for every redox system, the oxygen transport capacity for a reaction *i*, R_{OC}^i, is
248 defined as the mass fraction of the oxygen carrier being transferable as oxygen:

249 $$R_{OC}^i = \frac{m_o^i - m_r^i}{m_{oxid}^i} \quad (1)$$

250 m_o^i being the initial mass of the sample, m_r^i the mass of the reduced sample and m_{oxid}^i the sample mass
251 assuming oxidation under a determined condition. Distinction among m_o^i and m_{oxid}^i was done to consider
252 uncomplete oxidation of the oxygen carrier particles after calcination or oxidation stages, i.e. $m_o^i < m_{oxid}^i$. In

addition, the maximum oxygen transport capacity, $R^{i}_{OC,max}$, was calculated assuming that all material was oxidized to bixbyite.

By knowing the theoretical oxygen transport capacity, the oxygen carrier conversion was calculated using Eqs. 2 and 3 for reduction and oxidation, respectively.

$$X^{i}_{red\ red} = \frac{m_o - m}{R^{i}_{OC,th}\, m_{oxid}} \quad (2)$$

$$X^{i}_{ox} = \frac{m - m_r}{R^{i}_{OC,th}\, m_{oxid}} \quad (3)$$

For the oxygen uncoupling reaction, R^{ou}_{OC} is defined for reduction of bixbyite to spinel. When required, the presence of pyrophanite was also considered for the calculation of R^{ou}_{OC}. But for reduction with a fuel gas, R^{g}_{OC} is defined for reduction of the spinel phase to manganowüstite. The accumulated or total mass loss from bixbyite to manganowüstite is defined by $R^{t}_{OC} = R^{ou}_{OC} + R^{g}_{OC}$. Table 2 summarizes the theoretical and maximum values of these parameters, R^{ou}_{OC} and R^{t}_{OC}, for every oxygen carrier prepared in this work. The specific Mn-Fe composition of the different materials prepared in this work has been stablished to cover a wide range of Mn/(Mn+Fe) ratios on the basis of the phase diagram results shown in Figure 1. Theoretically, all the Ti substituted Mn-Fe mixed oxides materials show oxygen uncoupling, but FeTi7 does not show any interesting phase transformation unless a reducing gas was present.

Table 2. Oxygen transport capacity for gas-solid reactions, R^{t}_{OC}, and oxygen uncoupling, R^{ou}_{OC} at 950 ºC; the subscripts *"max"*, *"th"* and *"exp"* denote maximum, theoretical and experimental values, respectively.

	FeTi7	Mn28FeTi7	Mn55FeTi7	Mn66FeTi7	Mn87FeTi7	MnTi7
$R^{ou}_{OC,\max}$	0	3.1	3.1	3.6	3.6	3.6
$R^{ou}_{OC,th}$	0	3.1	3.1	3.6	2.8	0.47
$R^{ou}_{OC,\exp}$	0	0.47	1.5	1.3	1.9	0.38
$X_{ou,exp}$	-	0.15	0.47	0.36	0.67	0.81
$R^{t}_{OC,\max}$	9.3	9.4	9.4	9.4	9.4	9.4
$R^{t}_{OC,th}$	9.3	9.4	9.4	9.4	8.7	6.5
$R^{t}_{OC,\exp}$	4.0	4.8	7.3	7.4	7.8	6.2
$X_{t,exp}$	0.49	0.51	0.78	0.80	0.90	0.96

For all the cases, the maximum oxygen uncoupling capacities are within the 3.1-3.6 interval, and the

maximum oxygen transport capacities for gas-solid reaction are within the 9.3-9.4. The maximum oxygen carrier capacity achievement requires a suitable selection of the oxidation conditions in the air reactor, as shown in Figures 1(a) and 1(b). Thus, according to this Figure, decreasing the Mn content of the carrier will allow its fully oxidation to bixbyite at higher temperatures and/or lower partial pressure of O_2.

To evaluate the oxygen transport capability of prepared materials in this work, TGA experiments were carried out by oxidizing the samples at 950 ºC in air. Thus, the $R_{OC,th}^{ou}$ values are calculated by considering the stable phase after oxidation at 950 ºC in air. Under these conditions, Mn28FeTi7, Mn55FeTi7 and Mn66FeTi7 can be fully oxidized to bixbyite with 3.7, 7.4 and 12.6 vol.% O_2, respectively. Thus, both the maximum and theoretical ($R_{OC,th}^{ou}$ and $R_{OC,th}^{ou}$) were calculated to be 3.1 for Mn28FeTi7 and Mn55FeTi7, and 3.6 wt.% for Mn66FeTi7. The higher $R_{OC,\max}^{ou}$ and $R_{OC,th}^{ou}$ values for Mn66FeTi7 was due to the higher utilization of the oxygen in the formation of some pyrophanite, $MnTiO_3$, with respect to the spinel. This was the case also for $R_{OC,\max}^{ou}$ in Mn87FeTi7. But in this case, only a partial oxidation to bixbyite would be only possible in air at 950 ºC due to the miscibility gap observed for this material, and $R_{OC,th}^{ou}$ was correspondingly decreased to 2.8 wt.%. For MnTi7, bixbyite is not formed in any extension at 950 ºC in air. However, oxygen uncoupling was associated to the appearance of pyrophanite, $MnTiO_3$, which allows a certain capability of oxygen uncoupling for the spinel phase; see reaction R4.

Experimentally, any of the oxygen carriers reach their respective theoretical oxygen transport capability. The differences between $R_{OC,\exp}^{ou}$ and $R_{OC,th}^{ou}$ are in general increased as the Fe content is increased. Thus, the maximum conversion of Mn28FeTi7 is 0.15 and that of MnTi7 is 0.81. The oxygen carriers with intermediate Mn/(Mn+Fe) molar ratios (0.55-0.87 interval) showed intermediate conversion values.

The differences found in the $R_{OC,th}^{t}$ values, depending upon the Mn/(Mn+Fe) ratio, are also related to the phase transformations shown in Figure 1 when the oxygen partial pressure is varied. For the oxygen carriers with a Mn/(Mn+Fe) ratio between 0.66 and 1, the $R_{OC,th}^{t}$ values shows a decreased tendency as the Mn/(Mn+Fe) ratio is increased, whereas the $R_{OC,\max}^{t}$ values are kept unaltered. This issue is related to a progressive transformation of some of the mass in the oxidized state to spinel structures, with a more pronounced degree of conversion as the Mn content is increased, due to the specific oxidation conditions

298 considered in the air reactor (i.e. 950 ºC in air). This transformation counteracts the utilization of oxygen in
299 the system and consequently the $R^{t}_{OC,th}$ decreases with increased Mn/(Mn+Fe) ratios.

300 The experimental oxygen transport capacity for each oxygen carrier and operating condition was obtained
301 from reduction with H_2 in TGA; see Table 2. Only for MnTi7 the experimental $R^{t}_{OC,\exp}$ value lay within the
302 theoretical one, i.e. the solid conversion $X_{t,max}$ was close to unity; for the other carriers, the $R^{t}_{OC,\exp}$ values are
303 lower than the corresponding theoretical ones, with increased differences in $X_{t,max}$ as the Fe content in the
304 carrier is increased. This fact was related to the low degree of oxidation to bixbyite observed for these
305 materials; see $X_{ou,max}$ in Table 2. Nevertheless, the oxygen carriers with Mn/(Mn+Fe) molar ratios in the 55-87
306 interval showed the maximum experimental oxygen transport capacities.

307 **3.4. Reactivity results**

308 The evaluation of the oxygen carrier reactivity towards H_2, CO and CH_4, as well as its potential for oxygen
309 release have been done through isothermal redox cycles at 950 ºC in TGA. Also, the regeneration with
310 different partial pressures of oxygen is analyzed.

311 **3.4.1. Reactivity towards oxygen uncoupling**

312 To analyze the oxygen release, Figure 2 shows normalized conversion vs. time curves for the different oxygen
313 carriers when decomposed in N_2 and oxidized with air at 950 ºC. In general, the oxygen release rate is
314 increased as the Mn content in the oxygen carrier is increased; see Figure 2(a). Also the maximum oxygen
315 carrier conversion increased with the Mn content.

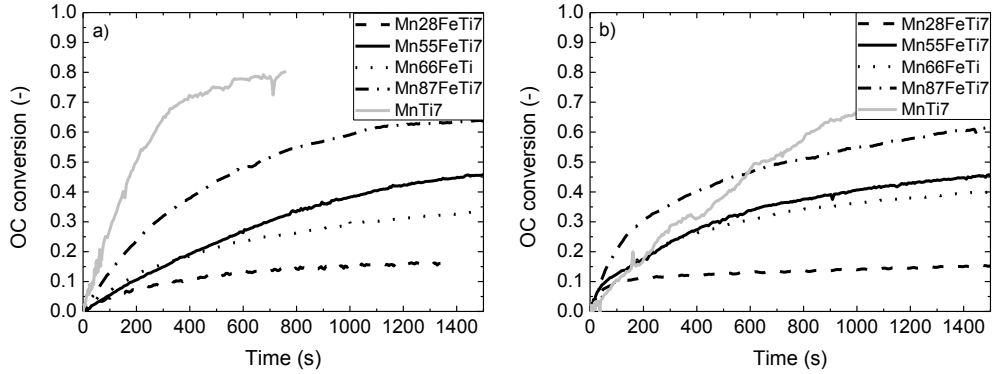

316
317 **Figure 2.** Solids conversion vs. time during (a) oxygen uncoupling in N_2, and (b) oxidation in air at 950 ºC.

318

319 However, the oxygen carrier conversion was limited by the conversion reached during the oxidation stage; see

Figure 2(b). For screening purposes, the oxidation was carried out at 950 ºC in air to force the formation of bixbyite as much as possible. The oxidation rate considerably slowed with the reaction progress, not achieving the full transport oxygen capacity at this temperature (950 ºC) for each redox system, in accordance with results shown in Table 2. The rate of oxygen transference per unit of mass, r_{O_2}, was a function of both the conversion-based reaction rate and the oxygen transport capacity:

$$r_{O_2}\left(\frac{kgO_2}{s\cdot kgOC}\right) = R_{OC,th}^{ou}\cdot\frac{dX_{ou}}{dt} \quad (4)$$

Figure 3 shows that the oxygen transference rate was higher for oxidation than for reduction, excepting for MnTi7. The oxygen transference rate during reduction, i.e. oxygen release, is in the $1\cdot10^{-5}$ to $4\cdot10^{-5}$ kgO_2/s per kg of oxygen carrier, with Mn87FeTi7 showing the highest reaction rate. These values can be compared to the oxygen transference rate values of about $1\cdot10^{-3}$ kgO_2/s per kg of highly reactive Cu-based materials [36,37] and about $3.5\cdot10^{-4}$ kgO_2/s per kg of promising $CaMnO_3$ based materials [31,38].

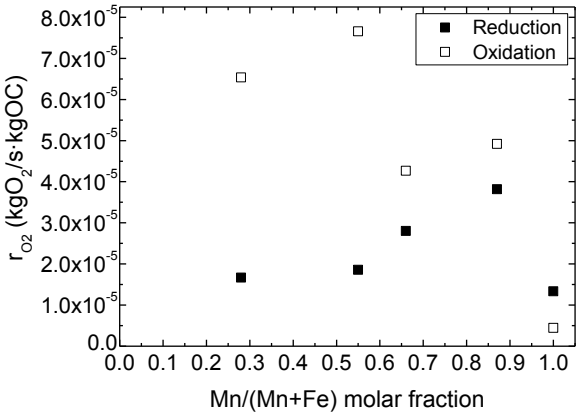

Figure 3. Instantaneous oxygen generation rate, r_{O_2}, for the different oxygen carriers at 950 ºC.

3.4.2. Reactivity towards reduction with H_2, CO and CH_4

Figure 4(a)-4(c) shows the conversion vs. time curves for the different oxygen carriers when reduced with CH_4, CO and H_2. All the oxygen carriers analyzed react faster with H_2 than with CO and CH_4, in spite of the concentration of H_2 is 3 times lower than the one corresponding to CO or CH_4. In addition, the reduction degree depended on the given Mn/(Mn+Fe) ratio and the reducing gas considered. Thus, decreasing the Mn content results into lower conversions, except for the FeTi7 carrier due to further reduction of magnetite to wüstite. Nevertheless, further reduction of magnetite is not of interest for CLC system based on

interconnected fluidized bed reactors [32], and only the part of the curve corresponding to reduction to Fe_3O_4, i.e. $X_{red} < 1$ for FeTi7, was here considered.

To go further into the evaluation of both reduction and oxidation reaction rates, the normalized rate index was calculated as [39]:

$$Rate\ index\ \left(\frac{\%}{min}\right) = 60 \cdot 100 \cdot R_{OC,th}^{t} \cdot \left(\frac{dX_i}{dt}\right)_{norm} \quad (5)$$

$\left(\frac{dX_i}{dt}\right)_{norm}$ being the normalized rate calculated for a partial pressure of 0.15 atm for fuel gases and 0.10 atm for oxygen.

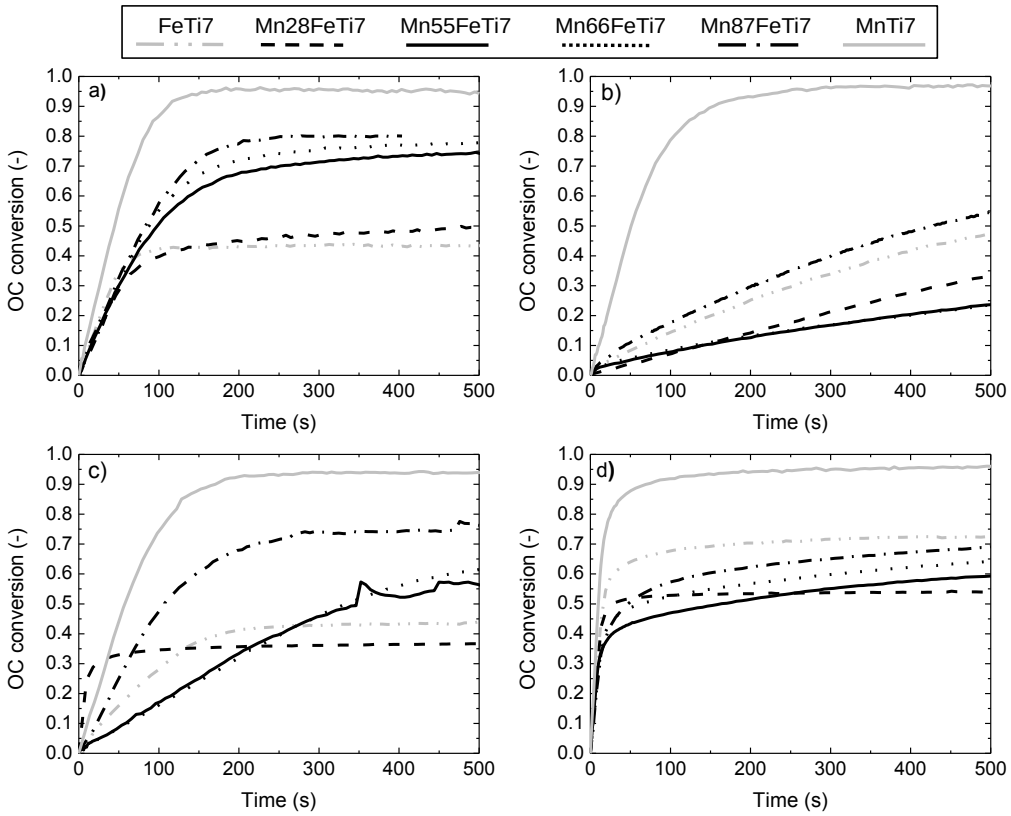

Figure 4. Oxygen carrier conversion with time during reduction with: a) H_2 (5% H_2 + 40% H_2O), b) CO (15% CO + 20% CO_2) and c) CH_4 (15% CH_4 + 20% H_2O), and oxidation with: d) air, at 950 ºC.

Rate index values obtained for reduction reactions are shown in Figure 5. Independently of the Mn/(Mn+Fe) ratio considered, the normalized rate index is considerably higher for reduction with H_2 than with CO or CH_4, as already noticed from the results shown in Figure 4. Considering the influence of the Mn/(Mn+Fe) ratio, the highest rate index values were found in the extremes, i.e. for Mn- or Fe-rich materials. In general, lower

values of rate index were found for materials with Mn/(Mn+Fe) ratios between 0.2 and 0.9, but interestingly these materials showed magnetic properties, In any case, rate index values for H_2 were similar to those of promising low cost materials for *i*G-CLC, e.g. ilmenite, Fe-ESF and Tierga Fe-ore [40,41], but lower rate index values were found for Mn-Fe mixed oxides with CH_4 and CO.

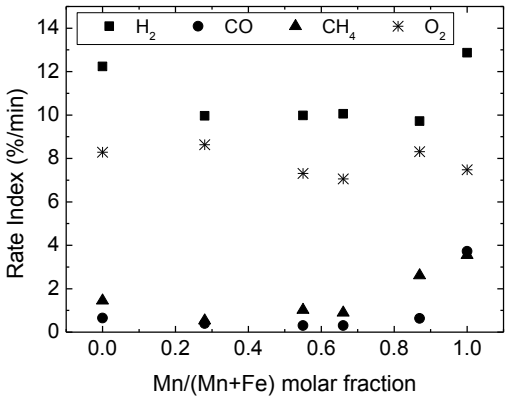

Figure 5. Normalized rate index for the reduction reactions of the different oxygen carriers with CH_4, CO and H_2, and their subsequent oxidation with air. T = 950 ºC, P_{ref} = 0.15 for reduction gases and P_{ref} = 0.10 for air.

The reaction kinetics and thermodynamic restrictions are very dependent on temperature. In order to analyze to what extent the reactivity are affected by the temperature, Figure 6(a) shows the normalized rate index during reduction with CH_4 at 850, 900 and 950 ºC. The effect of temperature on the reduction rate is low for the oxygen carriers with low Mn conten (Mn/(Mn+Fe)=0.28-0.66), and increases as the Mn concentration is increased (Mn/(Mn+Fe)≥0.87), with a promoted rate of reduction by increasing the reaction temperature. At 850 ºC the rate of reduction is considerably low for all the oxygen carriers studied and therefore higher temperatures (≥900 ºC) would be needed in the fuel reactor for a good performance of these redox systems.

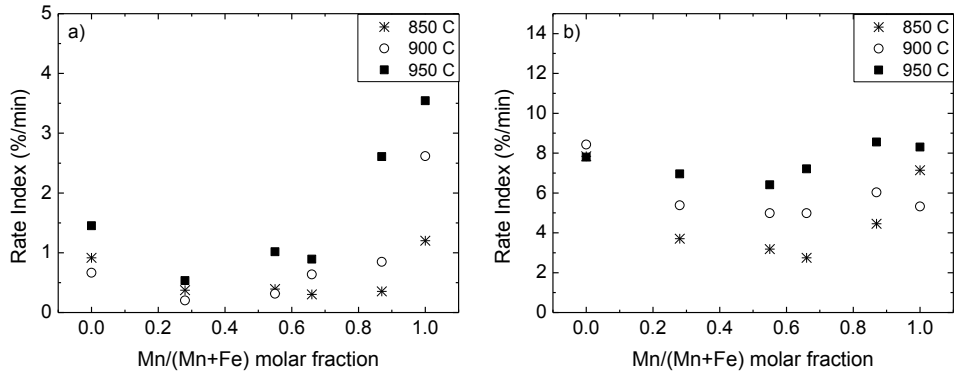

Figure 6. Normalized rate index for the (a) reduction and (b) oxidation reactions of the different oxygen carriers with CH_4 and air, respectively, at 850, 900 and 950 ºC. P_{ref} = 0.15 for CH_4 and P_{ref} = 0.10 for O_2.

3.4.3. Reactivity towards oxidation

The oxidation of manganowoustite to spinel phase is not problematic, and shows fast reaction kinetics for all the cases analyzed; see Figures 4(d) and 5. The most pronounced oxygen carrier regeneration is produced within the first 20 seconds. Eventually, the conversion reaches the value attained in the previous reduction cycle indicating the potential of these carriers for regeneration in the air reactor under these conditions. In addition, the oxidation rates are considerably high in the 850-950 ºC temperature range; see Figure 6(b). The rate index values for the oxidation of Mn-Fe mixed oxides are higher than those showed by other materials tested, such as ilmenite or Fe-ore [40,41]. Therefore, this step is not a determining factor when deciding the optimal composition of the oxygen carrier selected.

The oxidation of spinel to bixbyite phase following reverse of reaction R1, which is of interest in CLOU, is highly dependent on the reacting temperature and the oxygen concentration [29]. A preliminary evaluation was done using air for oxidation. Thus, oxidation in air was relatively high during the first 100 seconds and are almost independent of the Mn:Fe ratio considered; see Figure 2(b). In this case, the instantaneous oxygen generation rate (see Figure 3) shows the highest values for Mn/(Mn+Fe) ratios in the 0.28-0.55 interval and a minimum for the Mn rich material. However, the complete oxidation to bixbyite was not allowed in air at 950 ºC; see $X_{ou,exp}$ values in Table 2. Remarkable effect of the Mn:Fe ratio was found on conversion achieved, with higher maximum conversion values as the Mn content is increased. For the oxygen carrier with the highest Mn conten (MnTi7) the oxygen uncoupling observed is due to the spinel to pyrophanite transformation (reaction R3). Thus, these results indicate that after pyrophanite formation, the regeneration to spinel is possible.

Considering the effect of the oxygen concentration on the bixbyite regeneration, the phase diagram in Figure 1 shows that materials with Mn/(Mn+Fe) ratios higher than 0.55 are not able to oxidize to bixbyite with a 5 vol.% O_2 at 950 ºC. Thus, the air reactor should operate at lower temperatures for these materials. Thus, for

Mn55FeTi7 a temperature of 930 ºC is required to be completely oxidized to bixbyite, and a theoretical oxygen transport capacity of $R_{OC,th}^{ou}$ = 3.13 wt.% is exploitable for CLOU. But a temperature lower than 850 ºC is required to allow complete oxidation to bixbyite for Mn87FeTi7, while a temperature between 850 and 900 ºC would allow a partial oxidation of spinel to bixbyite due to the existence of a relevant miscibility gap. In this case, the usable oxygen transport capacity for CLOU, $R_{OC,th}^{ou}$, are 1.77 and 3.60 wt.% at 900 and 850 ºC, respectively. However, despite the favorable thermodynamics shown at 850 ºC, the regeneration of Mn87FeTi7 was not possible at this temperature due to slow kinetics. In this context, Figure 7 shows the conversion vs. time curves during oxidation in 5 vol.% O_2 at 930 ºC for Mn55FeTi7 and at 900 ºC for Mn87FeTi7. Mn87FeTi7 achieved higher conversion values for longer periods. But during the first seconds of the oxidation period (< 300 s), the oxidation rate of both carriers was almost similar. Considering that the mean residence time in the air reactor would be lower than 300 s, both Mn87FeTi7 and Mn55FeTi7 would be able to be oxidized in the air reactor with a similar behavior at their respective optimal temperatures.

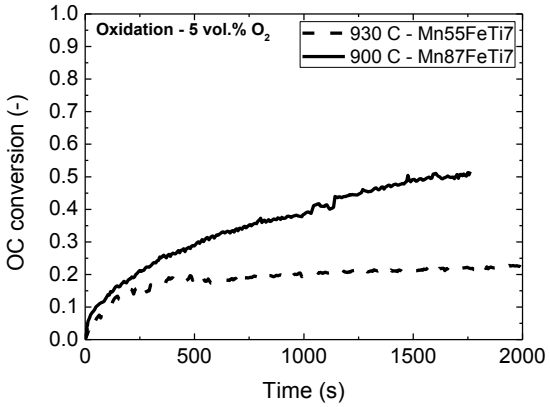

Figure 7. Conversion with time during oxidation with 5 vol.% O_2 at 900 ºC with Mn87FeTi7 and 930 ºC with Mn55FeTi7.

4. Discussion

A comprehensive evaluation of physical and chemical properties of the materials prepared with different Mn:Fe ratios is done regarding their capability to be used in *i*G-CLC and CLOU processes. All particles showed high enough crushing strength values (above 4 N in most of cases) to be used as oxygen carrier in the fluidized bed reactors of a CLC unit.

On the one hand, Mn28FeTi7, Mn55FeTi7 and Mn66FeTi7 showed high magnetic permeability values when

calcined at 1200 ºC. In addition, similar reactivity with fuel gases was found for these materials. If the oxygen uncoupling property is considered as well, bixbyite formation is favored for the Mn55FeTi7 material regarding results on oxygen transport capacity and regeneration reactivity. Therefore, under the same conditions for the rest of parameters, Mn55FeTi7 would be preferred among these materials to be used in the CLOU process.

On the other hand, oxygen carriers with Mn/(Mn+Fe) molar ratios in the 0.87-1 interval showed better reactivity towards CH_4, CO and H_2. However, only the Mn87FeTi7 showed soft magnetic properties after calcination at 1300 ºC; the MnTi7 carrier is not magnetic. The oxygen uncoupling property of this material is highly restricted by the oxidation conditions, as bixbyite formation requires a relatively high oxygen partial pressure and/or low oxidizing temperature. Therefore, the Mn87FeTi7 would be selected to be used in coal combustion in *i*G-CLC mode.

Following, the capabilities of selected materials, i.e. Mn55FeTi7 and Mn87FeTi7, to be used in *i*G-CLC and/or CLOU is assessed. The optimal conditions in the *i*G-CLC process would include the operation of the fuel reactor at the highest temperature possible. Considering the reactivity with fuel gases, Mn87FeTi7 shows a clear advantage compared to Mn55FeTi7 to be used in the *i*G-CLC mode. Mn87FeTi7 shows also higher reactivity and oxygen transport capacity for CLOU; see Table 2 and Figure 3. But some difficulties could be expected for the bixbyite regeneration in the air reactor compared to Mn55FeTi7, which is mandatory to take advantage of the oxygen uncoupling effect. Thus, more restricted conditions and lower temperature in the air reactor would be required for Mn87FeTi7 (see Figure 7), which would have also influence on a lower temperature in the fuel reactor due to the heat management of a CLC unit [42]. Considering the global reaction in the fuel reactor is exothermic when bixbyite-spinel redox system is considered for CLOU [17,43], the fuel reactor can operate at higher temperatures than the air reactor. Considering the optimal temperatures for the air reactor showed above, fuel reactor temperatures of 950 ºC for Mn87FeTi7 and at 980 ºC for Mn55FeTi7 seem reasonable. This option sacrifices the reaction rate with gases in order to exploit the oxygen uncoupling capability. To evaluate the performance of these oxygen carriers at these fuel reactor temperatures, Figure 8 shows the normalized rate index for the reduction with CH_4, H_2 and CO, as well as the instantaneous oxygen generation rate, for Mn87FeTi7 and Mn55FeTi7 at 950 ºC and 980 ºC, respectively. At their

446 respective optimal temperatures, both carriers exhibit similar reactivity towards reduction with H_2, CH_4, CO
447 and oxygen uncoupling.

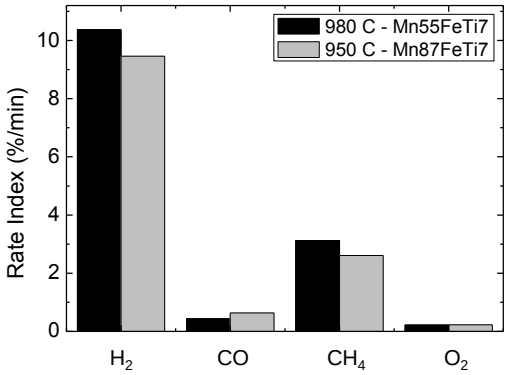

448
449 **Figure 8.** Normalized rate index (%/min) for the reduction of Mn55FeTi7 and Mn87FeTi7 with CH_4, H_2 and
450 CO, and the instantaneous oxygen generation rate (%/min), at 980ºC and 950ºC, respectively.

451

452 As a consequence of the results here shown, Mn55FeTi7 and Mn87FeTi7 materials are basically oxygen
453 carriers to be operated in *i*G-CLC mode. Note that reaction rate of oxygen generation by oxygen uncoupling
454 ($3.7 \cdot 10^{-5}$ s^{-1} for Mn55FeTi7 at 980ºC) are much lower than purely CLOU oxygen carriers such as Cu-based
455 materials [36,37]. However, even in this case, exploitation of the oxygen uncoupling capability would be very
456 beneficial, improving the performance of the CLC process via oxygen uncoupling in the so-called Chemical
457 Looping assisted by Oxygen Uncoupling (CLaOU) [19]. In addition, the Mn55FeTi7 oxygen carrier shows a
458 high magnetic permeability, μ = 8.3. Therefore, the ferromagnetic behavior showed by Mn55FeTi7 would
459 allow an easy separation from ashes in the CLC process with coal. In this context, the results of this study
460 settle Mn55FeTi7 as the most promising oxygen carrier for coal combustion via CLOU. Another option to be
461 considered is to operate the air reactor with a higher air excess, which would allow an increase of both fuel
462 and air reactors temperature. The adequacy of the utilization of oxygen uncoupling will take place in future
463 work on continuous plant operation.

464 **5. Conclusions**

465 The present work accomplishes a screening of the performance of Mn-Fe-Ti based oxygen carriers, prepared
466 with a fixed 7 % wt. TiO_2 and different Mn/(Mn+Fe) molar ratios, ranging from 0 to 1. Materials were
467 prepared through physical mixing following by pelletizing by pressure, calcining, crushing and sieving in the

100-300 particle size interval. The potential of the resultant oxygen carrier particles for the Chemical Looping Combustion process was determined theoretically through the prediction of the stable phases by thermodynamics and calculation of the oxygen transport capacity, and the subsequent comparison to solid phases found after characterization by XRD; and, experimentally through crushing strength, magnetic properties and redox reactivity analysis at suitable temperatures for the iG-CLC and CLOU process, using a thermogravimethic analyzer.

All the oxygen carriers prepared showed crushing strength values around 4-5 N. The magnetic permeability of the oxygen carriers increased as the Mn content decreased, but neither the FeTi7 carrier nor the MnTi7 showed any magnetic property.

The oxygen carriers with Mn/(Mn+Fe) molar ratios in the 0.55-0.87 interval showed the maximum values of either the oxygen uncoupling capacity and the oxygen transport capacity for gas-solid reactions. However, to take advantage of the oxygen uncoupling capability, the oxidation conditions should allow the formation of bixbyte in the air reactor. For highly Mn-rich materials, where this oxidation is very limited due to temperature limitations, oxygen uncoupling was also observed via the formation of pyrophanite in the presence of Ti.

Oxygen carriers with Mn/(Mn+Fe) molar ratios ≥ 0.87 showed the highest reactivity towards reduction gases (CH_4, CO and H_2) at 950ºC. However, oxygen carriers with lower Mn content (i.e. Mn/(Mn+Fe) = 0.55) showed similar reactivity during reduction at its optimal temperature, 980ºC.

Therefore, considering the balance between reactivity and magnetic properties, the oxygen carrier with Mn/(Mn+Fe) molar ratio of 0.55 would be very interesting for CLC with solids. In addition, regardless of MnTi7 did not show neither magnetic properties nor significant O_2 release, the good reactivity exhibited by this carrier with CO and H_2 would make it suitable for syngas combustion.

Acknowledgements

This work was partially supported by the Spanish Ministry for Economy and Competitiveness via the ENE2013-45454-R and ENE2014-56857-R projects, by the European Regional Development Fund (ERDF), and by the CSIC via the 2014-80E101 project. M. Abián acknowledges the MINECO and Instituto de Carboquímica (ICB-CSIC) for the post-doctoral grant awarded (FPDI-2013-16172).

References

[1] Mukherjeea S, Kumara P, Yangb A, Fennell P. Energy and exergy analysis of chemical looping combustion technology and comparison with pre-combustion and oxy-fuel combustion technologies for CO_2 capture. J Environ Chem Eng 2015;3:2104-2114.

[2] Lyngfelt A, Leckner B, Mattisson T. A fuidized-bed combustion process with inherent CO_2 separation; application of chemical-looping combustion. Chemical Engineering Science 2001;56:3101-3113.

[3] Adánez J, Abad A, Garcia-Labiano F, Gayan P, De Diego LF. Progress in chemical-looping combustion and reforming technologies. Progress in Energy and Combustion Science 2012;38:215-282.

[4] Berguerand N, Lyngfeld A. Chemical-looping combustion of petroleum coke using ilmenite in a 10 kW_{th} unit− high-temperature operation. Energy and Fuels 2009;23:5257-5268.

[5] Pérez-Vega R, Abad A, García-Labiano F, Gayán P, de Diego LF, Adánez J. Coal combustion in a 50 kW_{th} Chemical Looping Combustion unit: Seeking operating conditions to maximize CO_2 capture and combustion efficiency. International Journal of Greenhouse Gas Control 2016;50:80-92.

[6] Ohlemüller P, Busch J-P, Reitz M, Ströhle J, Epple B. Chemical-Looping Combustion of hard coal: Autothermal operation of a 1 MW_{th} pilot plant. Journal of Energy Resources Technology 2016;138:Article number 042203.

[7] Mendiara T, de Diego LF, García-Labiano F, Gayán P, Abad A, Adánez J. On the use of a highly reactive iron ore in Chemical Looping Combustion of different coals. Fuel 2014;126:239-249.

[8] Gu H, Shen L, Zhong Z, Niu X, Ge H, Zhou Y, Xiao S, Jiang S. NO release during chemical looping combustion with iron ore as an oxygen carrier. Chemical Engineering Journal 2015;264:211-220.

[9] Ma J, Zhao H, Tian X, Wei Y, Zhang Y, Zheng C. Continuous operation of interconnected fluidized bed reactor for chemical looping combustion of CH_4 using hematite as oxygen carrier. Energy and Fuels 2015;29:3257-3267.

[10] Linderholm C, Lyngfelt A, Cuadrat A, Jerndal E. Chemical-looping combustion of solid fuels - Operation in a 10 kW unit with two fuels, above-bed and in-bed fuel feed and two oxygen carriers,

manganese ore and ilmenite. Fuel 2012;102:808-822.

[11] Mendiara T, de Diego, LF, García-Labiano F, Gayán P, Abad A, Adánez J. Behaviour of a bauxite waste material as oxygen carrier in a 500W_{th} CLC unit with coal. International Journal of Greenhouse Gas Control 2013;17:170-182.

[12] Gayán P, Abad A, de Diego LF, García-Labiano F, Adánez J. Assessment of technological solutions for improving chemical looping combustion of solid fuels with CO_2 capture. Chemical Engineering Journal 2013;233:56-69.

[13] Mattisson T, Lyngfelt A, Leion H. Chemical-looping with oxygen uncoupling for combustion of solid fuels. International Journal of Greenhouse Gas Control 2009;3:11-19.

[14] Abad A, Adánez-Rubio I, Gayán P, García-Labiano F, de Diego LF, Adánez J. Demonstration of chemical-looping with oxygen uncoupling (CLOU) process in a 1.5kW_{th} continuously operating unit using a Cu-based oxygen-carrier. International Journal of Greenhouse Gas Control 2012;6:189-200.

[15] Adánez-Rubio I, Abad A, Gayán P, de Diego LF, García-Labiano F, Adánez J. Performance of CLOU process in the combustion of different types of coal with CO_2 capture. International Journal of Greenhouse Gas Control 2013;12:430-440.

[16] Adánez-Rubio I, Abad A, Gayán P, De Diego LF, García-Labiano F, Adánez J. Biomass combustion with CO_2 capture by chemical looping with oxygen uncoupling (CLOU). Fuel Processing Technology 2014;124:104-114.

[17] Rydén M, Leion H, Mattisson T, Lyngfelt A. Combined oxides as oxygen-carrier material for chemical-looping with oxygen uncoupling. Applied Energy 2014;113:1924-1932.

[18] Azimi G, Rydén M, Leion H, Mattisson T, Lyngfelt A. $(Mn_zFe_{1-z})_yO_x$ combined oxides as oxygen carrier for chemical-looping with oxygen uncoupling. AIChE Journal 2013;59:582-588.

[19] Pérez-Vega R, Abad A, Adánez J, de Diego LF, García-Labiano F, Gayán P. Development of a Mn-Fe-Ti based oxygen carrier in chemical looping combustion with coal. Int. Conf. Clean Coal Technologies, Krakow, Poland, 2015.

[20] Wang B, Gao C, Wang W, Zhao H, Zheng C. Sulfur evolution in chemical looping combustion of coal with $MnFe_2O_4$ oxygen carrier. Journal of Environmental Sciences 2014;26:1062-1070.

[21] Lambert A, Delquié C, Clémeneçon I, Comte E, Lefebvre V, Rousseau J, Durand B. Synthesis and characterization of bimetallic Fe/Mn oxides for chemical looping combustion. Energy Procedia 2009;1:375-381.

[22] Bhavsar S, Tackett B, Veser G. Evaluation of iron- and manganese-based mono- and mixed-metallic oxygen carriers for chemical looping combustion. Fuel 2014;136:268–279.

[23] Larring Y, Braley C, Pishahang M, Andreassen KA, Bredesen R. Evaluation of a mixed Fe−Mn oxide system for Chemical Looping Combustion. Energy and Fuels 2015;29:3438-3445.

[24] Azimi G, Leion H, Rydén M, Mattisson T, Lyngfelt A. Investigation of different Mn-Fe oxides as oxygen carrier for chemical-looping with oxygen uncoupling (CLOU). Energy and Fuels 2013;27:367-377.

[25] Shafiefarhood A, Stewart A, Li F. Iron-containing mixed-oxide composites as oxygen carriers for Chemical Looping with Oxygen Uncoupling (CLOU). Fuel 2015;139:1–10.

[26] Novák P. Contribution of octahedrally co-ordinated Mn^{3+} ion to magnetic torque. Czechoslovak Journal of Physics 1971;21:1198-1212.

[27] Bakare PP, Gupta MP, Date SK, Sinha APB. Structural, magnetic and Mössbauer studies on $MnxFe_{3-x}O_4$ ($0 \leqslant x \leqslant 1$). Proceedings of the Indian Academy of Sciences - Chemical Sciences 1984;93:1349-1359.

[28] Mostafa NY, Hessien MM, Shaltout AA. Hydrothermal synthesis and characterizations of Ti substituted Mn-ferrites. Journal of Alloys and Compounds 2012;529:29-33.

[29] Pérez-Vega R, Abad A, de Diego LF, García-Labiano F, Adánez J. Development of $(Mn_{0.77}Fe_{0.23})_2O_3$ Particles as Oxygen Carrier for Coal Combustion with CO_2 capture via *in-situ* Gasification Chemical Looping Combustion (*i*G-CLC) aided by Oxygen Uncoupling (CLOU). Submitted for publication, 2016.

[30] Pérez-Vega R. Captura de CO_2 en la combustion de carbon con transportadores sólidos de oxígeno (PhD. Thesis). Instituto de Carboquímica (ICB-CSIC), Zaragoza, Spain, 2016.

[31] de Diego LF, Abad A, Cabello A, Gayán P, García-Labiano F, Adánez J. Reduction and oxidation kinetics of a $CaMn_{0.9}Mg_{0.1}O_{3-\delta}$. Industrial and Engineering Chemistry Research 2014;53:87-103.

[32] Abad A, García-Labiano F, de Diego LF, Gayán P, Adánez J. Reduction kinetics of Cu-, Ni-, and Fe-based oxygen carriers using syngas (CO + H_2) for chemical-looping combustion. Energy and Fuels 2007;21:1843-1853.

[33] Bale CW, Bélisle E, Chartrand P, Decterov SA, Eriksson G, Hack K, Jung I-H, Kang Y-B, Melançon J, Pelton AD, Robelin C, Petersen S. FactSage thermochemical software and databases – recent developments. CALPHAD 2009;33:295-311.

[34] Cabello A, Gayán P, García-Labiano F, De Diego LF, Abad A, Adánez J. On the attrition evaluation of oxygen carriers in Chemical Looping Combustion. Fuel Processing Technology 2016;148:188-197.

[35] Rydén M, Moldenhauer P, Lindqvist S, Mattisson T, Lyngfelt A. Measuring attrition resistance of oxygen carrier particles for chemical looping combustion with a customized jet cup. Powder Technology 2014;256:75-86.

[36] Gayán P, Adánez-Rubio I, Abad A, de Diego LF, García-Labiano F, Adánez J. Development of Cu-based oxygen carriers for Chemical-Looping with Oxygen Uncoupling (CLOU) process. Fuel 2012;96:226-238.

[37] Adánez-Rubio I, Gayán P, Abad A, García-Labiano F, de Diego LF, Adánez J. Kinetic analysis of a Cu-based oxygen carrier: Relevance of temperature and oxygen partial pressure on reduction and oxidation reactions rates in Chemical Looping with Oxygen Uncoupling (CLOU). Chemical Engineering Journal 2014;256:69-84.

[38] Abad A, García-Labiano F, Gayán P, de Diego LF, Adánez J. Redox kinetics of $CaMg_{0.1}Ti_{0.125}Mn_{0.775}O_{2.9-\delta}$ for Chemical Looping Combustion (CLC) and Chemical Looping with Oxygen Uncoupling (CLOU). Chemical Engineering Journal 2015;269:67-81.

[39] Johansson M, Mattisson T, Lyngfelt A. Comparison of oxygen carriers for Chemical-Looping Combustion. Thermal Science 2006;10:93-107.

[40] Abad A, Adánez J, Cuadrat A, García-Labiano F, Gayán P, de Diego LF. Kinetics of redox reactions of ilmenite for chemical-looping combustion. Chemical Engineering Science 2011;66:689-702.

[41] Mendiara T, Pérez R, Abad A, de Diego LF, García-Labiano F, Gayán P, Adánez J. Low-cost Fe-based oxygen carrier materials for the iG-CLC process with coal. 1. Industrial and Engineering Chemistry Research 2012;51:16216-16229.

[42] Abad A, Adánez J, García-Labiano F, de Diego, LF, Gayán P, Celaya J. Mapping of the range of operational conditions for Cu-, Fe-, and Ni-based oxygen carriers in chemical-looping combustion.

Chemical Engineering Science 2007;62:533-549.

[43] Mattisson T. Review Article, Materials for Chemical-Looping with Oxygen Uncoupling. ISRN Chemical Engineering 2013;Article ID 526375.